Biomimetic Mineralisation of Noble Metal Nanocluster

ARTICLE *in* BIOMACROMOLECULES · SEPTEMBER 2003

Impact Factor: 5.75 · DOI: 10.1021/bm034003q · Source: PubMed

2 AUTHORS, INCLUDING:

David W Wright
Vanderbilt University
142 PUBLICATIONS **2,714** CITATIONS

Articles

Biomimetic Mineralization of Noble Metal Nanoclusters

Joseph M. Slocik and David W. Wright*

Department of Chemistry, VU Station B 351822, Vanderbilt University, Nashville, Tennessee 37235-1822

Received January 3, 2003; Revised Manuscript Received April 17, 2003

A number of biological systems have developed highly orchestrated detoxification mechanisms toward the bioreduction and mineralization of noble metals. These systems incorporate small peptides and proteins as nucleation sites for metal binding and nanocluster stabilization. Herein, we present the use of biologically relevant ligands ranging from single amino acids (histidine, imidazole, and cysteine) to linear peptides (glutathione and a histidine rich peptide) in the stabilization of a variety of noble metal surfaces (Au^0, Ag^0, Pt^0, and Cu^0). As a result, the different nanocluster/ligand combinations offered a broad range of sizes and stabilitites. The peptide coat also affords a unique functional handle for the formation of larger assemblies. Using Ni chelation and immunomolecular approaches, strategies for the assembly of nanocluster heterostructures were investigated.

Introduction

Many biological systems exert exquisite control over the formation of biogenic metal nanoclusters through a combination of concerted mechanisms involving bioaccumulation, reduction, and mineralization processes to protect themselves from the deleterious effects of metal toxicity. Examples of biosynthetically produced Ag^0 and Au^0 nanocrystals can be found in such organisms as *Pseudomonas stuzeri*,[1] *Verticillium sp.*,[2] *Lactobacillus* strains,[3] *Pedomicrobium*-like bacteria,[4] *Medicagos sativa*,[5] and *Fusarium oxysporum*.[6] The bacterium of *Pseudomonas stutzeri* produces tetragonal shaped silver crystals of ∼200 nm within the periplasmic space.[1] *Pedomicrobium*-like bacteria were discovered to produce naturally exquisite lacelike networks of gold at a quality of 24 carats anchored on gold placar deposits.[4] Recently, extracellular reduction and synthesis of Au^0 nanoclusters was achieved with *Fusarium oxysporum* fungal cells through the release of proteins into solution that enzymatically reduced Au^{3+} to Au^0 and stabilized the nanocluster against aggregation through protein-surface binding.[6] Understanding these highly specialized natural processes for nanocluster formation provides insight into new approaches for the synthesis of bio-inspired materials.

Noble metals afford highly functional materials with properties such as wavelength selective plasmon absorption resonances, conductivity, and catalytic activity. As a result, the synthesis and applicability of noble metal nanoclusters has generated much interest. Current reported strategies for the synthesis of noble metals primarily involve modifying the nanocluster surfaces of Au^0, Ag^0, and Pt^0 with various alkylthiol derivatives,[7−9] alkylamine groups,[9,10] and poly(vinylpyrrolidone)[11] polymers. Unfortunately, most of these ligands are simply aimed at stabilizing the nanocluster surface. There is, however, a growing interest in the programmed assembly of individual nanoparticles into large structures. One approach is the use of appropriately selected biological macromolecules to serve as the organizing element, providing not only the stabilizing ligand but also a recognition element between nanoparticles. Examples of such approaches include the utilization of DNA elements in a nanoparticle coat,[12] combinatorially selected peptide presenting viruses,[13] antibodies,[14,15] and designed bifunctional proteins[16] capable of associating dissimilar materials to form assemblies over multiple length scales.

One paradigm employed by biological systems for nanocluster synthesis is the expression of small peptides/proteins which serve as binding templates/nucleation sites for metal ions and then serve to stabilize the nanocluster core against continued aggregation. An exemplar for the utilization of peptides to control the formation of nanoclusters is the encapsulation of CdS clusters by phytochelatin peptides.[17,18] Recently, a small peptide associated with silver binding and reduction was identified using a combinatorial phage display peptide library.[19] The isolated 12-mer peptide biomimetically produced Ag^0 nanocrystals of 60−150 nm with a variety of crystal morphologies. Recently, we have reported that the histidine-rich epitope (HRE) from the histidine-rich protein II (HRP II) of *Plasmodium falciparum* (AHHAHHAAD) was capable of stabilizing a variety of nanoclusters, including Au^0 and Ag^0.[20] Herein, we examine the systematic stabilization of noble metal nanoclusters (Au^0, Ag^0, Pt^0, and Cu^0) by a collection of biologically relevant ligands ranging from single amino acid donors to linear 9-mer peptides. In total, these different metal−ligand combinations yielded

* To whom correspondence should be addressed. Phone: 1-615-322-2636. Fax: 1-615-343-1234. E-mail: David.Wright@vanderbilt.edu.

10.1021/bm034003q CCC: $25.00
Published on Web 06/28/2003

20 nanoclusters with a broad scope of sizes and stability. Furthermore, the peptide coat provides a unique functionality on the nanocluster surface. We have investigated Ni-chelation and immunomolecular recognition of surface stabilizing peptides to form complex cluster heterostructures.

Experimental Section

Materials. Stock solutions (0.1M) of $HAuCl_4$, K_2PtCl_4, $AgNO_3$, and $CuCl_2$ (Aldrich) were dissolved with doubly deionized water. Stock solutions (0.1 M) of L-histidne (Aldrich), L-cysteine (Sigma), imidazole (Aldrich), and reduced glutathione (Acros) were prepared in doubly deionized water. The HRE peptide was previously synthesized and purified following standard Fmoc protocols and purification techniques.[21]

Synthesis of Au^0 and Ag^0 Nanoclusters. The synthesis is modified from previous literature procedure of Slocik et al.[20] In 10 individually labeled 10 mL vials, 100 μL of Au^{3+} or Ag^+ was added with 200 μL of each ligand stock solution (His, Imid, HRE, Cys, and GSH) along with a rice sized stir bar under anaerobic conditions and in the absence of light. To the vials containing Ag^+ and Au^{3+} complexes of histidine, imidazole, and HRE, 5.00 mL of doubly deionized water was added. To the vials of Au^0-(Cys), Au^0-(GSH), Ag^0-(Cys), and Ag^0-(GSH), 5.00 mL of Tris buffer (0.1 M, pH 8.6) was added. The metal−ligand precursor complexes were allowed to form for 15 min with stirring. To each vial, 100 μL of 0.1 M $NaBH_4$ was added dropwise. The reductions were carried out for 4 h at which point the clusters were completely formed. Immediately, the crude reaction products were purified by repeated precipitation with cold absolute ethanol. The isolated clusters were dissolved in a minimal amount of water and lyophilized on a Labconco freedry system for characterization.

Synthesis of Cu^0 and Pt^0 Nanoclusters. In 10 glass vials, 100 μL of Cu^{2+} or Pt^{2+} was added with 200 μL of each stock solution of ligand (His, Imid, HRE, Cys, and GSH) and diluted with 5.00 mL of Tris buffer. After 15 min of stirring, 100 μL of $NaBH_4$ was slowly added dropwise and left for 4 h. Purification and isolation was performed similar to Au^0 and Ag^0 above.

Nanoparticle Charcterization. Nanoclusters were characterized by UV−vis, XRD, TEM, EDS, and IR. Powder X-ray diffraction scans were obtained on a Scintag X_1 θ/θ automated powder diffractometer with a Cu target, a Peltier-cooled solid-state detector, and a zero background Si(510) sample support. Particle sizes were determined by using the DMSNT software (version 1.30c) provided by Scintag which fitted the data with a profile function to extract the full-width-at-half-maximum (fwhm) values. Average crystallite sizes were calculated from Scherrer's equation.

Clusters were also examined on a Phillips CM 20T transmission electron microscope (TEM) operating at 200 kV. TEM samples were prepared by pipetting one drop of the cluster solution in water onto a 3 mm diameter nickel grid or copper grid covered with holey carbon film as a substrate (SPI supplies) and quickly removed from droplet to dry. Particle size distributions were determined by manually measuring particle diameters from the bright-field micrographs. The TEM was fitted with an EDAX DX-4 package for energy-dispersive X-ray spectrometry (EDS). Samples were tilted at 15° for analysis at 200 kV.

UV−vis spectroscopy was done on an Agilent 8453 photodiode array spectrometer with sample concentrations $\sim 2 \times 10^{-5}$ M. Infrared spectra of nanoclusters in a KBr pellet were obtained on a Mattson Genesis series FTIR spectrometer.

Nickel Chelation Binding. The surface HRE coats of the purified clusters, Ag^0-(HRE), Au^0-(HRE), Pt^0-(HRE), Cu^0-(HRE), and Au^0-(His) as a control, were examined via a binding assay with a commercially available 96 well plate coated with a nickel chelate (Xenopore). The plates did not require blocking prior to use and were used as received. A solution of each purified cluster at a concentration of $\sim 10^{-5}$ M was prepared in Tris buffer and an initial UV−vis spectrum was taken in a 50 μL quartz cell. 300 μL of each cluster solution was pipetted into three wells and incubated for 2 h with shaking. After 2 h, the UV−vis spectrum from each well was examined.

Antibody Recognition Assays. The HRE stabilized clusters of Cu^0-(HRE) and Pt^0-(HRE) were assayed with the commercially available malaria test kit, ***Para***sight F, following the previously reported procedure.[20] Antibody recognition of the glutathione clusters (Ag^0-(GSH), Au^0-(GSH), Pt^0-(GSH), and Cu^0-(GSH)) was achieved by magnetic separation of the antibody-nanocluster heterostructure. An antibody/(anti-antibody) magnetic complex was initially formed by titrating 200 μL of BioMag Goat anti-Rat IgG Fc specific (Polysciences, Inc., lot #502374, concentrated 5 $\times 10^8$ magnetic particles/mL) and 100 μL of Rat polyclonal to glutathione antiserum[22] (Abcam ab6447-100, lot #171001, diluted 1/1000 in 0.1 M Tris buffer pH 8.6) in a 96 polypropylene well plate (Nunc). At 30 min intervals for 2 h, the well plate was gently swirled. After 2 h, the magnetic antibody coupled complex was separated on a BioMag 96 well plate separator (Polysciences, Inc., small neodymium magnets arranged in a plastic frame) for 15 min. The excess antibody was removed from the magnetic particles by removing the supernatant. This was followed by washing the separated particles with 300 μL of 0.1 M Tris buffer pH 8.6. In three empty wells, 50 μL of the complete magnetic/antibody conjugate was added with 100 μL of the selected purified nanocluster along with 200 μL of Tris buffer. After a 2 h reaction period, the particles were magnetically separated and repeatedly washed with Tris buffer to remove unbound nanoclusters. A drop of the suspended particles was placed on a nickel or copper TEM grid and quantitated by EDS.

Results and Discussion

Nanoparticle Synthesis and Characterization. The set of stabilizing biomolecules for Au^0, Ag^0, Pt^0, and Cu^0 consisted of the thiol based donors of L-cysteine (Cys)[23] and tripeptide glutathione (GSH, γ-ECG)[24] and amine based ligands of imidazole (Imid), L-histidine (His), and a histidine

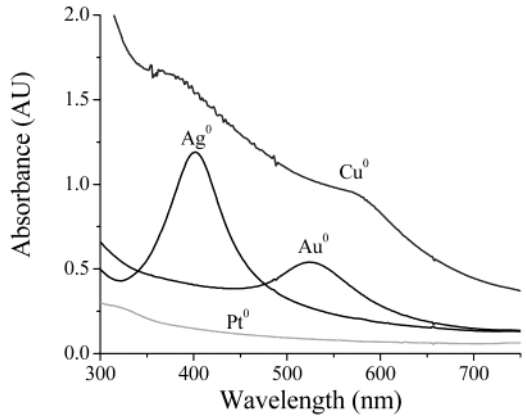

Figure 1. UV−vis absorption spectra of the HRE encapsulated noble metal nanoclusters.

Table 1. Nanocluster Characterization[a]

nanocluster	plasmon abs. (nm)	XRD sizes (nm)	unit cell a (Å)	TEM sizes (nm)
Au^0-(Imid)	NA-ppt	2.8	4.07	6.6 ± 2.2
Au^0-(His)	518	3.1	4.05	4.1 ± 1.7
Au^0-(HRE)	524	5.0	4.09	9.5 ± 3.0
Au^0-(Cys)	511	1.9	4.07	3.8 ± 1.0
Au^0-(GSH)	512	5.1	4.05	4.5 ± 1.2
Ag^0-(Imid)	422 (br.)			26.5 ± 7.6
Ag^0-(His)	393 (br.)	13.2	4.09	10.0 ± 3.0
Ag^0-(HRE)	402	7.4	4.09	11.2 ± 4.0
Ag^0-(Cys)	434 (br.)	11.3	4.20	6.1 ± 2.8
Ag^0-(GSH)	486	6.5	4.34	8.6 ± 3.5
Pt^0-(Imid)	320	4.4	3.93	4.0 ± 1.1
Pt^0-(His)	270	2.7	3.92	3.4 ± 1.0
Pt^0-(HRE)	317	7.9	3.91	3.1 ± 0.8
Pt^0-(Cys)	NA (br.)	12.4	3.89	16.9 ± 8.4
Pt^0-(GSH)	NA (br.)	14.9	3.89	17.0 ± 6.2
Cu^0-(Imid)	575			6.3 ± 1.5
Cu^0-(His)	571			6.9 ± 2.4
Cu^0-(HRE)	574			7.9 ± 3.5
Cu^0-(Cys)	398			3.5 ± 0.8
Cu^0-(GSH)	363			9.7 ± 4.3

[a] NA, not apply; ppt, precipitate; br, broad.

rich epitope peptide (HRE) with the sequence of AHHAHHAAD. As a consequence of the significant differences between Lewis acidity and basicity for some metal/ligand combinations and the extent to which a particular ligand associates with a metal surface, the synthesis of the complete matrix of encapsulated zerovalent nanoclusters with the desired properties of good crystallinity, stability, and optical characteristics was challenging. Nevertheless, these differences in ligand stabilization provide important insight into the biomimetic requirements of nanocluster formation.

The synthesized nanoclusters displayed a range of optical properties (Figure 1). The ligand set of HRE, His, Cys, and GSH, produced Au^0 clusters with plasmon resonances ranging from λ_{max} 512−524 nm (Table 1). The analogous set of Ag^0 clusters exhibited absorbance maxima between λ_{max} 393−486 nm with differing degrees of peak broadening. The monodentate ligands (Imid, His, and Cys) yielded broad asymmetrical peaks due to ineffectual stabilization of the Ag^0 nanocluster surface resulting in multiple size domains. This broadening effect was previously reported for Ag^0-(Cys) clusters under similar reaction conditions.[23] It should be noted that all imidazole functionalized clusters suffered from agglomeration and concomitantly precipitated from solution over the time course of the reaction. The set of Pt^0 clusters failed to show distinguishable plasmon absorption bands due to the electronic and dielectric properties of platinum. Theoretically, the spectra are associated with wide absorption bands which decay in the direction of longer wavelengths.[25] This was manifest in the respective spectra of the ligand stabilized Pt^0 clusters as being featureless and paralleled the spectrum of polyacrylate stabilized Pt^0 sols.[25] For the Cu^0 nanoclusters, the choice of surface ligand shifted the plasmon absorption resonance band of copper from 375 nm for the thiol ligands to 573 nm for amine stabilized clusters. The later is consistent with previously reported copper nanoclusters encapsulated in a poly(amidoamine) dendrimer structure.[26]

Differences in the crystallinity of the noble metal nanoclusters as a function of the stabilizing ligand were noted in XRD and TEM analysis. From XRD studies, the peptide and amino acid stabilized clusters of Au^0, Ag^0, and Pt^0 exhibited a significant degree of crystallinity, confirmed by the major diffractions of (100), (200), (220), and (020) for a face centered cubic lattice structure (see the Supporting Information). Representative average sizes were calculated from these diffractions following Scherrer's equation (Table 1**)**. Further, the unit cell parameter, *a*, was determined for each sample providing a statistical assessment of the experimental fit with the theoretical unit cell value **(**Table 1**)**. In contrast, the Ag^0-(Cys), Ag^0-(GSH), Pt^0-(GSH), and Pt^0-(Cys) nanoclusters produced poor diffraction patterns. The poor crystallinity of the Ag^0-(Cys), Ag^0-(GSH), Pt^0-(Cys), and Pt^0-(GSH) is consistent with the interactions of certain thiol containing ligands with metal surfaces. These interactions promote a remodeling of surface atoms that diverge from an idealistic lattice structure into a more disorganized nonperiodic form. For example, it was reported that platinum clusters with an octanethiol surface were heavily disordered at the outer shell with only the core being crystalline.[23] Interestingly, the cysteine and glutathione clusters of Au^0 exhibited strong diffractions indicative of a more ordered interface, similar to other reported gold−alkanethiol nanoclusters.[27] The isolated Ag^0-(Imid) and all of the Cu^0 nanoclusters showed no discernible diffraction pattern. In the case of the later, this is likely a result of decomposition with molecular oxygen or the formation of an oxide layer (see below). Tomalia et al. have reported that exposure to molecular oxygen will sufficiently oxidize Cu^0 clusters stabilized within PAMAM dendrimers to a green Cu^I complex leading to a terminal Cu^{II} complex.[26,28]

When examined by TEM (Figure 2), the metal nanocluster populations appeared spherical ranging in size from averages of 3.0−27.0 nm in diameter with a monomodal size distribution **(**Table 1**)**.[29] Clear differences in dispersity and aggregation were observed in these populations as a function of the capping ligand, indicating a balance between the stability of the metal−ligand precursor complex and the propensity to form metal−metal bonds during nanocluster growth upon reduction. For example, the set of Ag^0 nanoclusters exhibited the largest range of sizes from 6.1 to 26.5

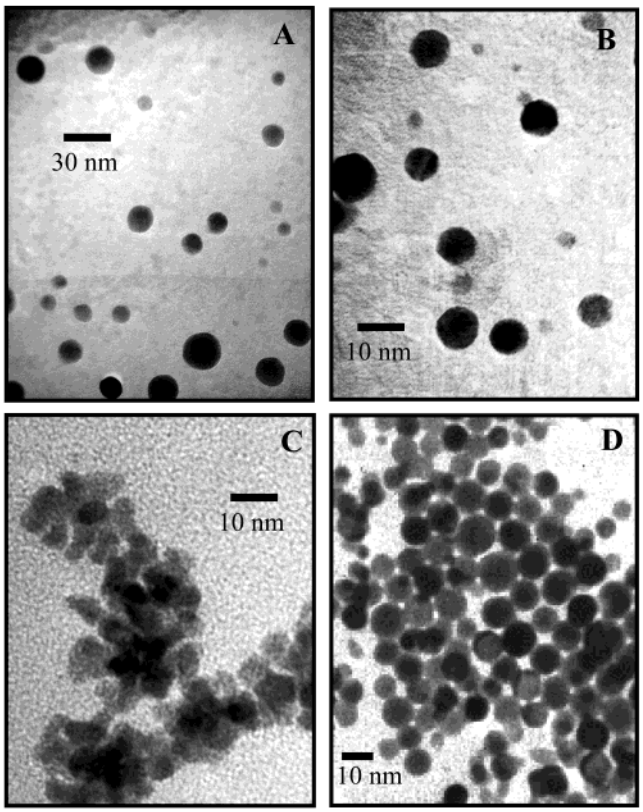

Figure 2. Representative TEM micrographs of nanocluster populations. (A). Cu^0-(GSH) 310 000X (B). Ag^0-(Cys) 750 000X (C). Pt^0-(His) 750 000X (D). Au^0-(HRE) 750 000X.

nm with the different ligands. For these nanoclusters, the smallest nanoparticles were obtained with the amines, whereas the largest were stabilized by thiol moieties. In contrast to the predominantly spherical morphologies of the nanoclusters, the Pt^0 nanoclusters displayed signs of aggregation (Figure 2C). Similar aggregation behavior of platinum nanoclusters has been previously observed with mercaptosuccinic acid, citrate, or polymer as the stabilizing ligand.[30] In these examples, incomplete coverage of ligand molecules on the particle surface results in exposed metal surface contact points leading to subsequent particle aggregation.[30] The imidazole clusters were irregularly shaped with signs of agglomeration (see the Supporting Information).

The collection of purified clusters exhibited a characteristic pattern of vibrational stretching frequencies implicating the presence of ligands residing on the nanocluster surface (see the Supporting Information). IR analysis of cysteine and glutathione bound to the nanocluster surface was evinced by the absence of the S−H stretch at 2554 and 2522 cm^{-1} from the free ligand spectra and the relatively unshifted carboxylate stretches.[23] An exception was Cu^0-(Cys) which shows a weak S−H stretching vibration, suggesting the possible involvement of the ligand's amine moiety in surface coordination as well. In the spectra of all of the glutathione encapsulated nanoclusters, the peptide amide I band is shifted by 20 cm^{-1} as previously reported by Kimura et al.[32]

Analysis of the imidazole stabilized clusters showed a disappearance of multiple N−H stretching bands relative to free imidazole in the region of 3118−2617 cm^{-1}. Previous studies have attributed the loss of these vibrations as indicative of deprotonation of N−H and formation of a

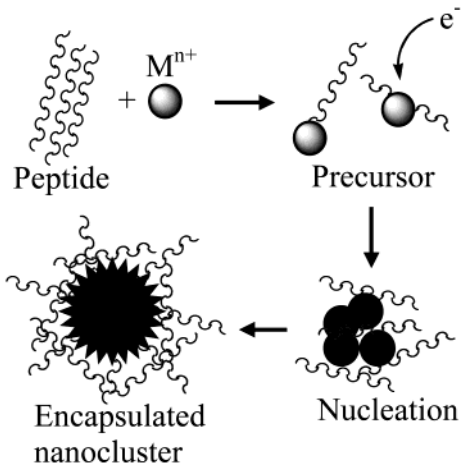

Figure 3. Model for synthesis of peptide encapsulated nanoclusters. Synthesis begins with complexation of metal ion to ligand, followed by borohydride reduction of metal complex, nucleation, and finally formation of peptide-stabilized nanocluster.

metal−imidazole bond on the metallic silver surface.[33] Alternately, interactions with the dielectric field at the nanoparticle surface has been reported to broaden vibrational features, thereby, reducing their intensity.[23,31] Similarly, the histidine analogues displayed a loss of N−H bands. In addition to imidazole binding, the carboxylate group of the histidine amino acid was perturbed to varying extents as measured by shifts in frequency and broadening of the asymmetrical and symmetrical CO_2^- stretches.[34,35] Notably, the asymmetrical CO_2^- stretch of Ag^0-(His) displayed a $\Delta\nu$ +10 cm^{-1} suggesting a possible metal−carboxylate interaction. As with histidine encapsulated nanoclusters, the HRE peptide stabilized clusters demonstrated diminished N−H stretching bands relative to free imidazole vibrations. HRE peptide stabilized clusters also showed broad IR peaks attributed to the amide I and II bands of the peptide backbone shifted from the free ligand spectra. Pt^0-(HRE) and Cu^0-(HRE) contained amide bands shifted by 20 cm^{-1} indicating an extensive hydrogen bonding network occurring near the surface. These results are consistent with vibrational data from other peptide encapsulated nanoclusters.[20]

Consistent with the synthesis and characterization data, a likely scheme for biomimetic nanocluster formation is shown in Figure 3. The amino acid or peptide ligand interacts with metal ion to form a ligand-stabilized precursor complex. Upon addition of reductant, small nuclei are rapidly formed. The amino acid or peptide ligands adhere to growing nuclei leading to a lower surface energy of the crystal lattice, thereby, accelerating nanocluster growth (see the Supporting Information). Eventually, the surface of the growing nanocluster is passivated by the ligand coat, terminating nanoparticle growth. This scheme is analogous to those previously suggested for the peptide encapsulation of CdS[36] and ZnS.[37] Brown et al. have extended this paradigm by showing that face specific adsorbing peptides can additionally modulate the morphology of gold nanoclusters.[38] Recently, Djalali et al. have shown that the monodispersity of this reaction can be significantly improved by using the insoluble Au^{3+} precursor, $ClAuPMe_3$.[39] Although the reaction takes significantly longer because the peptide must leach the metal ion from the insoluble complex (5 days vs 4 h), only the

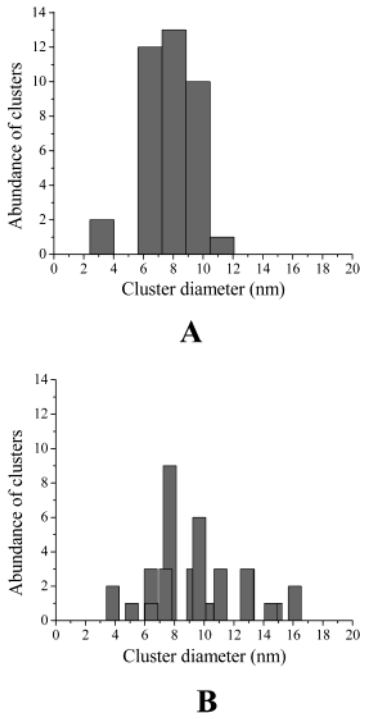

Figure 4. Dispersity of nanoclusters obtained by different synthetic strategies for Au^0-(HRE). (A) Method of Djalali et al. utilizing insoluble $ClAuPMe_3$. (B) Method of Slocik et al. using soluble $HAuCl_4$.

precursor peptide−metal ion complex is formed. Consequently, the reduction is more controlled, producing a narrower distribution of nanoclusters (Figure 4). Ultimately, if appropriate insoluble metal ion precursors were available for the entire range of desired clusters, this approach may result in significant improvements in the monodispersity of biomimetically synthesized nanoparticles.

Nanocluster Surface Recognition. The rationale behind the peptides used in this study was not only to examine their ability to stabilize a nanocluster surface but more importantly to provide a functional handle on the nanoparticle surface. To explore the resulting surface functionality of the HRE peptide stabilized nanoclusters, a nonspecific histidine binding assay on a nickel chelating surface was performed (Figure 5). The coated well plate surface provided by Xenopore was in the form of a covalently linked nickel nitrilotriacetic acid complex which provided two open coordination sites for histidine binding. The maximal adsorption isotherm provided by Xenopore estimates a ∼12% binding efficiency using a 22-mer model peptide with 5 histidine residues bound at the N terminus.[40] Upon addition of Ag^0-(HRE) or Au^0-(HRE) to the nickel chelating surface, 9.5% and 5.1% of the clusters bound to the nickel surface corresponding to 79% and 42.4% binding efficiency, respectively. This mode of interaction is indicative of the presence of free histidines on the nanocluster surface that are not involved in nanocluster surface coordination. The lower binding efficiencies displayed by these particles are likely due to steric effects resulting from the dispersity of nanocluster sizes and number of histidines in a favorable conformation for interaction. Binding of Cu^0-(HRE) and Pt^0-(HRE) was inconclusive because of their inherently weak plasmon absorption resonances, but a loss in absorbance was noted. In contrast, the Au^0-(His) nanocluster control showed no signs of binding, suggesting a

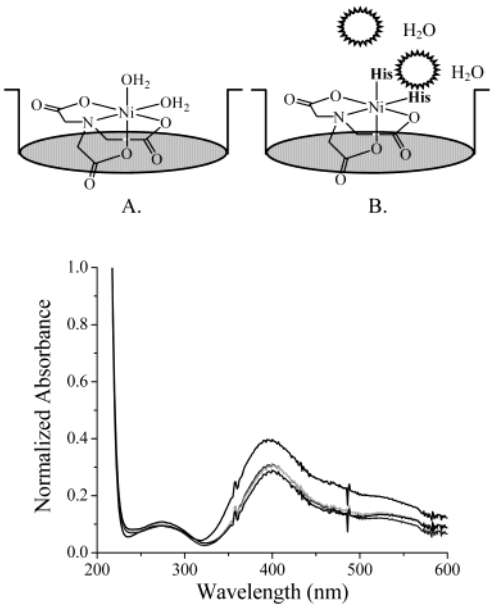

Figure 5. Ni-chelation binding assay. (A) Nickel chelate surface of a microplate well. (B) Chelation of available histidine residues from the HRE peptide surface of a nanocluster. (spiked circles = HRE peptide encapsulated nanoclusters). The absorbance spectrum below represents a loss in absorbance of Ag^0-(HRE) as a result of binding to the nickel surface in three different trials.

ligand coat of coordinated imidazole side chains to the cluster's surface. Consideration of the possible metal-coordination modes of the HRE peptide sequence of A*H*HA*H*HAAD suggests two sets of histidine residues on opposing peptide faces (Histidines 2/5 and 3/6). Consequently, the unbound histidines are accessible for bidentate nickel chelation. Given the number of peptide ligands bound to these nanoclusters (70−110 peptides), the HRE encapsulated clusters represent the nanoparticle equivalent of a histidine-tagged protein.

Antibody Recognition of Nanoclusters. Just as the stabilizing peptides can provide additional coordination sites on a nanoparticle surface, they may also present additional molecular recognition motifs. Previously, we reported that the HRE peptide surfaces of Ag^0-(HRE) and Au^0-(HRE) constituted an immunomolecular interface in which monoclonal antibodies to HRP II of *P. falciparum* recognized the peptide encapsulated nanoparticles.[20] Utilizing a simple commercially available ***Para***sight F test kit for malaria, Pt^0-(HRE) and Cu^0-(HRE) clusters exhibited similar immunoreactivity (see the Supporting Information). Positive recognition suggests that the HRE peptide adopts a conformation that is easily recognized by the antigen binding site of the antibody.[20] The recognition is facilitated by the fact that there are multiple peptide epitopes presented on the nanoparticle surface.

Analogous to the immunoreactive HRE stabilized clusters, an immunomolecular interface was used to assemble a superparamagnetic Fe_3O_4−IgG (BioMag)/noble metal nanocluster heterostructure. BioMag particles are mechanically milled iron oxide cores coated with silane and covalently attached to goat anti-rat IgG antibodies used in immunoassays or cellular separations. To assemble the immunomolecular construct, the functionalized BioMag particles were reacted with Rat polyclonal IgG antibodies that were specific

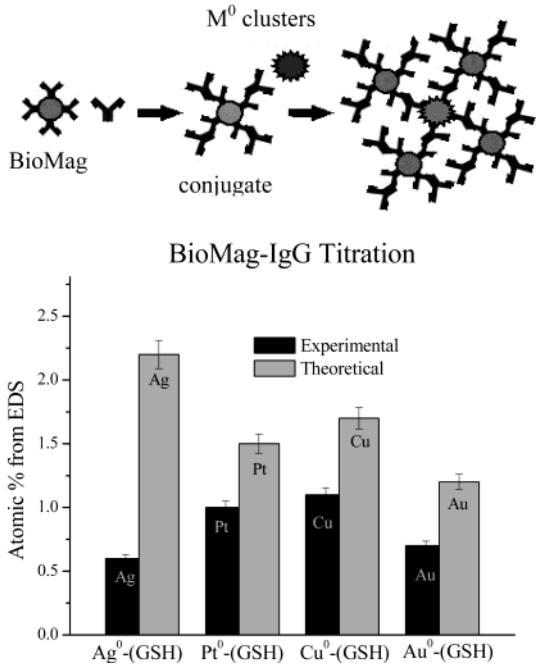

Figure 6. Antibody mediated heterocluster assembly. The assay begins with conjugation of Fe_3O_4 IgG (BioMag) particles to polyclonal antibodies to glutathione, followed by titration to glutathione stabilized nanoclusters, and separation of the BioMag/nanocluster heterostructure by a magnetic field of small neodymium magnets. The histogram represents the atomic % of metal (nanocluster core) from EDS that bound to the antibody/(anti-antibody) BioMag complex. Theoretical values were determined by calculating the number of iron atoms in the Fe_3O_4 core of 11.9 nm BioMag particles, assuming a binding stoichiometry of (5−25) BioMags per nanocluster, and the number of metal atoms in the glutathione clusters.

to glutathione **(**Figure 6). The antibody/(anti-antibody) conjugated BioMag (BioMag-IgG) assembly was then titrated with purified glutathione encapsulated clusters (Ag^0-(GSH), Au^0-(GSH), Cu^0-(GSH), and Pt^0-(GSH)). After formation of the BioMag/nanocluster heterostructure, the particles were separated by a magnetic field (neodymium magnets) from excess unbound nanoclusters and quantitated by energy-dispersive X-ray spectrometry (EDS) as to the atomic composition.

EDS analysis of the antibody linked assemblies revealed the presence of the iron-oxide particles, as well as the glutathione encapsulated noble metal clusters. For example, Pt^0-(GSH)/BioMag-IgG assay revealed an Lα X-ray emission for Pt with a peak area equivalent to 1.0 atomic % (weight % of 3.4) and an intense Kα emission for iron (atomic % 99.0, weight % 96.6). These values are above the average limit of detection by EDS which has been determined to be 0.12 wt % for oxygen.[41] Additionally, EDS of the negative binding control of BioMag-IgG/Ag^0-(Cys) did not detect the presence of Ag^0 atoms consistent with a lack of antibody recognition and minimal nonspecific binding (see the Supporting Information).

According to the manufacturer's specifications, 20−80 BioMag particles with an average particle size of 1 μm will bind a cell for effective magnetic separation. Sampling of several lots of BioMag particles by TEM revealed an actual size of 11.9 ± 4.9 nm with aggregates up to 1 μm. Given that nanoclusters are several orders of magnitude smaller than cells, the glutathione encapsulated nanoclusters could accommodate a range of particles from 5 BioMag particles bound to its surface to as many as 25 indirectly associated BioMag particles bound through BioMag−BioMag interactions. Based on these assumptions, an 11.9 nm Fe_3O_4 BioMag particle binding in a 5:1 stoichiometry with a 4.5 nm Au^0-(GSH) cluster will theoretically yield approximately 2.81×10^3 Au^0 atoms (1.6 atomic %) and 1.79×10^5 total iron atoms (98.4 atomic %). In the case of the larger 8.6 nm Ag^0-(GSH) cluster associated with an estimated 25 BioMag, the EDS spectrum shows 1.96×10^4 atoms of Ag^0 (2.2 atomic %) and 8.96×10^5 atoms of iron (97.8 atomic %). The experimental titration values indicative of antibody recognition range from 25 to 68% of the theoretical values (Figure 6). The discrepancy between complete and actual antibody recognition can arise from inefficiencies in two different recognition events: (1) recognition between the anti rat-IgG antibody and the rat glutathione antibody or (2) recognition between the rat glutathione antibody and the glutathione encapsulated nanocluster. Additionally, the latter recognition event will also be greatly effected by the confirmation of the peptide on the nanocluster surface. Regardless, the absolute immunomolecular mediated recognition efficiency of 25−60% is significantly higher than the constrained surface coordination-exchange recognition of the histidine-tagged nanocluster approach described above.

Conclusions

The stabilization of a variety of nanocluster surfaces was achieved with a diverse group of biomolecular ligands. The mineralization begins with the formation of a metal ion−peptide precursor complex. Upon addition of reductant, nucleation beings with rapid growth of the nanoparticle. Growth is terminated upon encapsulation of the growing cluster by surface stabilizing peptides. The properties of the surface ligand influenced the final properties of the nanocluster such as cluster sizes, stability, and crystallinity. The resulting dispersity and/or aggregation of the isolated nanoparticles from this study is reminiscent of the variety of biological derived noble metal minerals observed in nature.[1−6]

The peptide ligands provide a unique functionality to the surface of these biomimetic nanoclusters. Not only do they have side chains involved in coordination to the nanoparticle surface but they maintain residues directed toward the bulk solution. Consequently, the nanocluster surfaces may be programmed with small peptide recognition elements amenable to the controlled formation of larger assemblies. Two assembly strategies were investigated: Ni-chelation and antibody recognition. Au^0 and Ag^0 nanoclusters stabilized by a histidine-rich peptide (HRE) demonstrated the ability to bind to Ni−NTA coated plates, much like a His-tagged protein. Epitope presenting nanoparticles were linked via antibody binding to assemble Fe_3O_4−IgG/noble metal nanocluster heterostructures. Based on several limiting models of interaction, antibody-epitope recognition achieved efficacies of 25−68%. These proof of concept demonstrations highlight how biomolecularly programmed components can provide the requisite building blocks for the assembly of new biologically inspired nanomaterials.

Acknowledgment. This work was supported by the National Science Foundation CAREER award (CHE-0196540).

Supporting Information Available. EDS data and representative spectra of antibody mediated heterocluster assembly (1 pg). XRD of nanoclusters (1 pg). UV−vis absorbance spectra of nickel chelating assay (1 pg). UV−vis absorbance spectra of nanoclusters. Infrared spectra of purified nanoclusters (1 pg). Table of vibrational assignments (1 pg). UV−vis absorbance spectra of Cu^0-(GSH) oxidation (1 pg). TEM micrographs of representative nanoclusters. (A) Cu^0-(GSH), (B) Cu^0-(GSH), (C) Pt^0-(His), (D) Ag^0-(Cys), (E) Cu^0-(HRE), (F) Au^0-(Imid) (2 pgs). Histograms of the TEM size distributions of individual nanocluster populations (2 pgs). TEM size histogram of a BioMag sample (1 pg). Results of the ***Para***sight F test for antibody recognition of the HRE surface (1 pg). UV−Vis spectra obtained for the oxidation of Cu^0 nanoclusters (1 pg). Representative plot of nanocluster formation as a function of time (1 pg). This material is available free of charge via the Internet at http://pubs.acs.org.

References and Notes

(1) Klaus, T.; Joerger, R.; Olsson, E.; et al. *Proc. Natl. Acad. Sci.* **1999**, *96*, 13611−13614.
(2) Mukherjee, P.; Ahmad, A.; Mandal, D.; et al. *Angew. Chem., Int. Ed.* **2001**, *40*, 3585−3588.
(3) Nair, B.; Pradeep, T. *Cryst. Growth Design* **2002**, *2*, 293−298.
(4) Mann, S. *Nature* **1992**, *357*, 358−360.
(5) Gardea-Torresdey, J. L.; Parsons, J. G.; Gomez, E. *Nano Lett.* **2002**, *2*, 397−401.
(6) Mukherjee, P.; Senapati, S.; Mandal, D.; et al. *ChemBioChem* **2002**, *5*, 461−463.
(7) Vijaya Sarathy, K.; Kulkarni, G. U.; Rao, C. N. R. *Chem. Commun.* **1997**, 537−538.
(8) Dassenoy, F.; Phillippot, K.; Ould Ely, T.; et al. *New J. Chem.* **1998**, 703−711.
(9) Fu, X.; Wang, Y.; Wu, N.; Gui, L.; Tang, Y. *J. Colloid Interface Sci.* **2001**, *243*, 326−330.
(10) Leff, D. V.; Brandt, L.; Heath, J. R. *Langmuir* **1996**, *12*, 4723−4730.
(11) Ayyappan, S.; Srinivasa Gopalan, R.; Subbanna, G. N.; Rao, C. N. R. *J. Mater. Res.* **1997**, *12* (2), 398−401.
(12) Storhoff, J. J.; Mirkin, C. A. *Chem. Rev.* **1999**, *99*, 1849−1862.
(13) Whaley, S. R.; English, D. S.; Hu, E. L.; Barbara, P. F.; Belcher, A. M. *Nature* **2000**, *405*, 665−668.
(14) Mamedova, N. N.; Kotov, N. A.; Rogach, A. L.; Studer, J. *Nano Lett.* **2001**, *1*, 281−286.
(15) Wang, S.; Mamedova, N.; Kotov, N. A.; Chen, W.; Studer, J. *Nano Lett.* **2002**, *2*, 817−822.
(16) Brown, S. *Nano Lett.* **2001**, *1*, 391−394.
(17) Dameron, C. T.; Winge, D. R. *Nature* **1989**, *338*, 596−597.
(18) Dameron, C. T.; Winge, D. R. *Inorg. Chem.* **1990**, *29*, 1343−1348.
(19) Naik, R. R.; Stringer, S. J.; Agarwal, G.; Jones, S. E.; Stone, M. O. *Nature Mater.* **2002**, *1*, 169−172.
(20) Slocik, J. M.; Moore, J. T.; Wright, D. W. *Nano Lett.* **2002**, *2*, 169−172.
(21) Ziegler, J.; Chang, R. T.; Wright, D. W. *J. Am. Chem. Soc.* **1999**, *121*, 2395−2400.
(22) Amara, A.; Coussemacq, M.; Geffard, M. *Brain Res.* **1994**, *659*, 237−242.
(23) Mandal, S.; Gole, A.; Lala, N.; et al. *Langmuir* **2001**, *17*, 6262−6268.
(24) Schaaff, T. G.; Knight, G.; Shafigullin, M. N.; Borkman, R. F.; Whetten, R. L. *J. Phys. Chem. B* **1998**, *102* (52), 10643−10646.
(25) Ershov, B. G.; Sukhov, N. L. *Rus. J. Phys. Chem.* **2001**, *75*, 1303−1306.
(26) Balogh, L.; Tomalia, D. A. *J. Am. Chem. Soc.* **1998**, *120*, 7355−7356.
(27) Maye, M. M.; Zheng, W.; Leibowitz, F. L.; Ly, N. K.; Zhong, C. *Langmuir* **2000**, *16*, 490−497.
(28) For the peptide encapsulated clusters, the stabilizing ligand influences the extent of oxidation for the different clusters to the terminal Cu^{2+}-$(Ligand)_n$ in the following order: Cu^0-(Imid) > Cu^0-(GSH) > Cu^0-(His) > Cu^0-(HRE) (see the Supporting Information).
(29) When comparing experimentally determined average particle diameter, TEM estimates represent number averaged values, whereas particle diameter estimates from XRD peak width measurements are volume-weighted. Consequently, the presence of a fraction of particles having diameters much smaller or larger than the number average values will give disproportionately smaller or larger particle sizes by XRD.
(30) Chen, S.; Kimura, K. *J. Phys. Chem. B.* **2001**, *105*, 5397−5403.
(31) Leff, D. V.; Brandt, L.; Heath, J. R. *Langmuir* **1996**, *12*, 4723−4730.
(32) Chen, S.; Yao, H.; Kimura, K. *Langmuir* **2001**, *17*, 733−739.
(33) Xue, G.; Dai, Q.; Jiang, S. *J. Am. Chem. Soc.* **1988**, *110*, 2393−2395.
(34) Deacon, G. B.; Huber, F.; Phillips, R. J. *Inorg. Chim. Acta* **1985**, *104*, 41−45.
(35) Carlson, R. H.; Brown, T. L. *Inorg. Chem.* **1966**, *5* (2), 268−277.
(36) Spreitzer, G.; Whitling, J. W.; Madura, J. D.; Wright, D. W. *J. R. Soc., Chem. Commun.* **2000**, 209−210.
(37) Kho, R.; Torres-Martinez, C. L.; Mehra, R. K. *J. Colloid Interface Sci.* **2000**, *227*, 561−566.
(38) Brown, S.; Sarikaya, M.; Johnson, E. *J. Mol. Biol.* **2000**, *299*, 725−735.
(39) Djalali, R.; Chen, Y.-F.; Matsui, H. *J. Am. Chem. Soc.* **2002**, *124*, 13660−13661.
(40) XENOPORE Corp, Technical Notes, Hawthorne NJ.
(41) Love, G.; Scott, V. D. *J. Microscopy* **2001**, *201*, 1−32.

BM034003Q